Supplement of Atmos. Chem. Phys., 25, 1307–1331, 2025
https://doi.org/10.5194/acp-25-1307-2025-supplement

Atmospheric Chemistry and Physics
Open Access
EGU

Supplement of

Regional modeling of surface solar radiation, aerosol, and cloud cover spatial variability and projections over northern France and Benelux

Gabriel Chesnoiu et al.

Correspondence to: Isabelle Chiapello (isabelle.chiapello@univ-lille.fr)

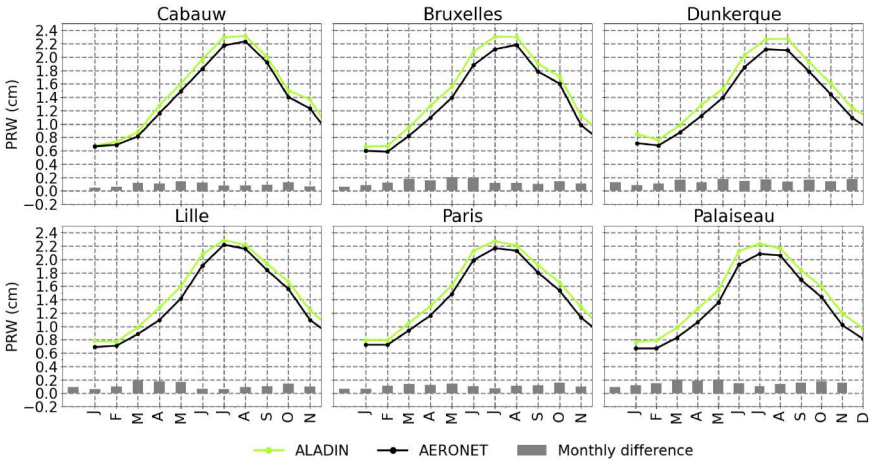

Figure S1. Comparisons of the monthly means (2010-2020) of integrated precipitable water (PRW, in cm) simulated by ALADIN in hindcast mode (green lines) with coincident photometric measurements (black lines) for the six AERONET measurement sites located in the BNF region. The monthly mean differences between the simulations and ground measurements are represented as grey columns.

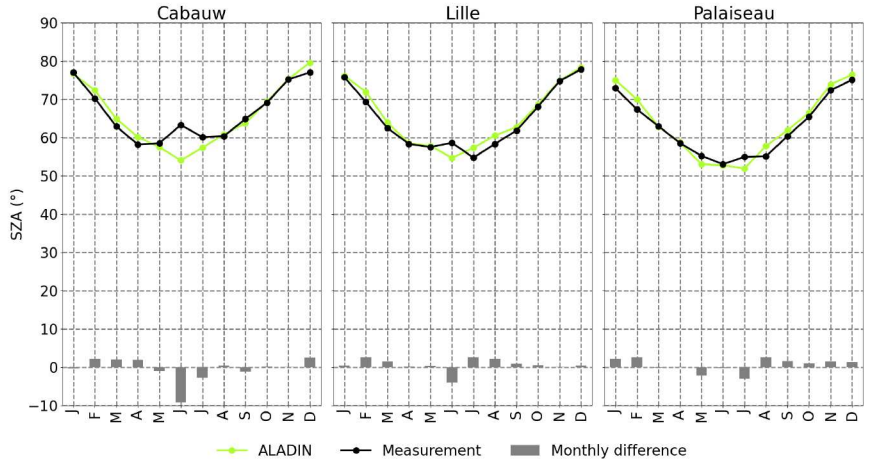

Figure S2. Comparisons of the monthly means (2010-2020) of measured (black lines) and simulated in hindcast mode (green lines) daytime average solar zenith angle under clear-sky (in degrees) conditions for the three irradiance measurements stations located within the BNF region. The monthly mean differences between the simulations and ground measurements are represented as grey columns.

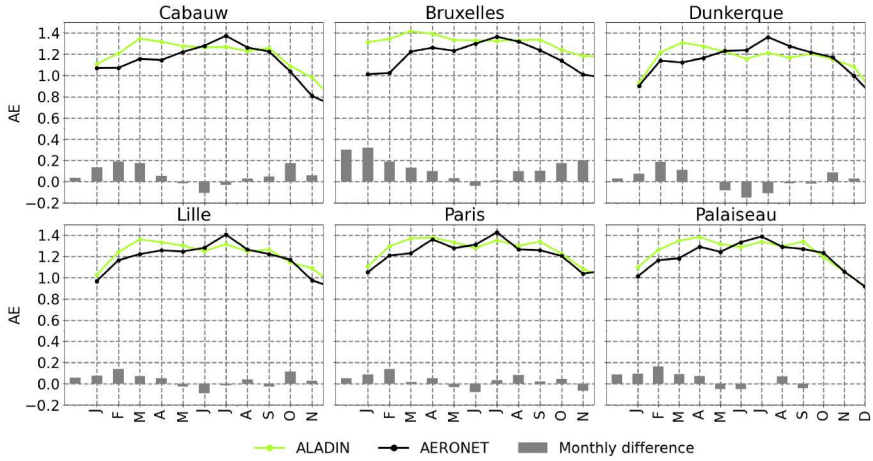

Figure S3. Comparisons of the monthly means (2010-2020) of Ångström exponent between 440 and 870 nm simulated by ALADIN in hindcast mode (green lines) with coincident photometric measurements (black lines) for the six AERONET measurement sites located in the BNF region. The monthly mean differences between the simulations and ground measurements are represented as grey columns.

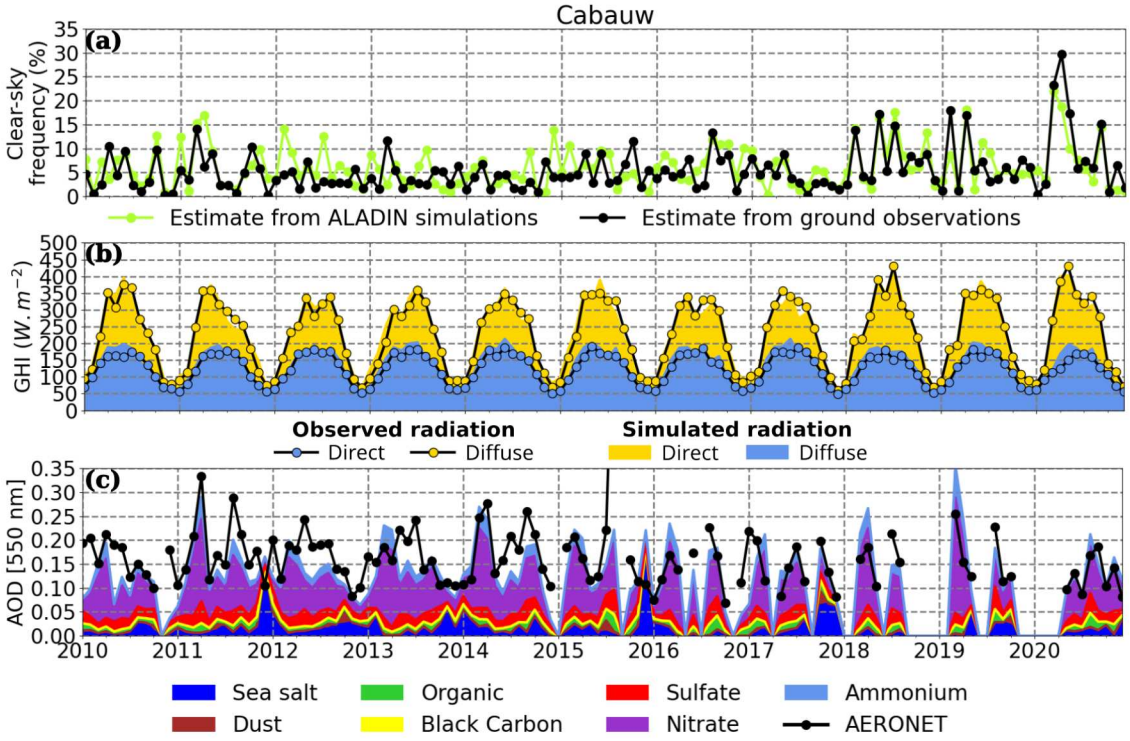

Figure S4. Comparisons of the simulated and measured monthly time series of daytime average (a) clear-sky frequency, (b) all-sky irradiances and (c) AOD at 550 nm in Cabauw over the period 2010-2020. In panel (a), green lines correspond to estimates based on ALADIN hindcast simulations (CLT < 3.5%), while black lines represent estimates based on the cloud-screening algorithm of Long and Ackerman (2000) applied to the surface solar irradiance measurements. In panel (b), ALADIN hindcast simulations and ground-based measurements are represented as colored areas and lines, respectively. The total height of each area or line represents the monthly average global irradiance, which is the sum of the direct (in yellow) and diffuse (in blue) components. In panel (c), ALADIN hindcast simulations of the seven aerosol types are represented as colored areas, while AERONET photometric measurements are depicted by thick black lines. As photometric measurements are only reliable in the absence of clouds in the direction of the Sun, they may not be representative of all-sky conditions. Hence, for consistency, monthly mean values derived from ALADIN hourly AOD simulations are limited to simulations coincident with measured hourly (diurnal) averages.

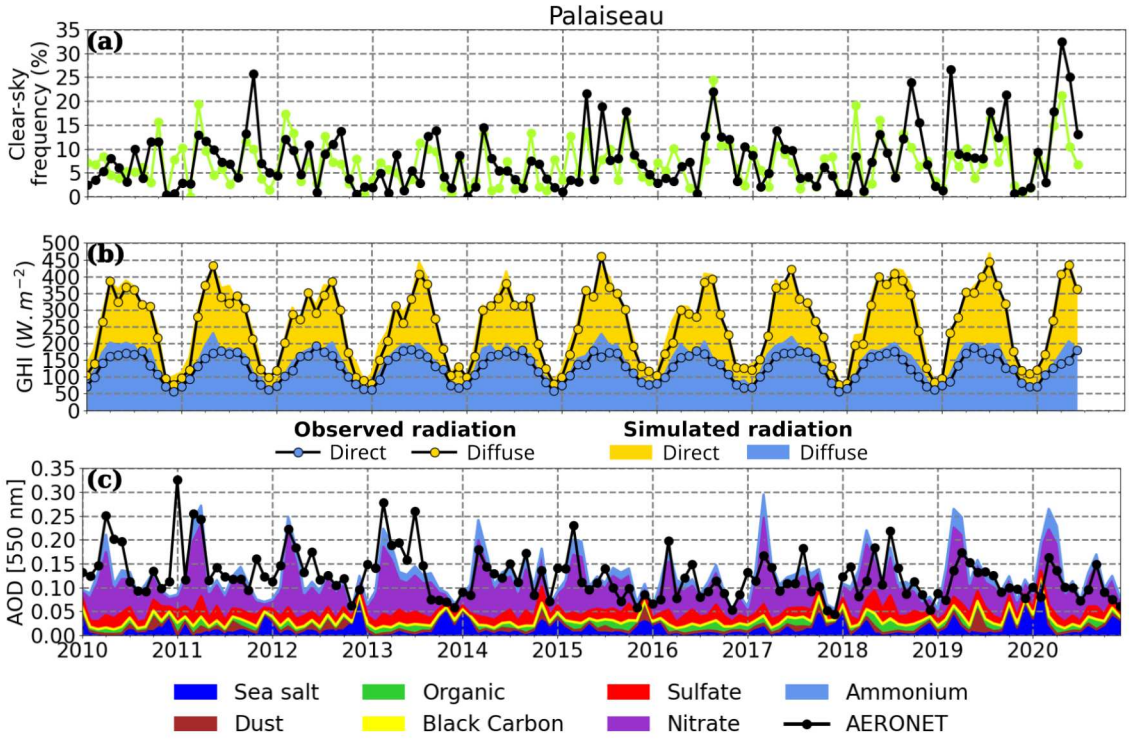

Figure S5. Comparisons of the simulated and measured monthly time series of daytime average (a) clear-sky frequency, (b) all-sky irradiances and (c) AOD at 550 nm in Palaiseau over the period 2010-2020. In panel (a), green lines correspond to estimates based on ALADIN hindcast simulations (CLT < 3.5%), while black lines represent estimates based on the cloud-screening algorithm of Long and Ackerman (2000) applied to the surface solar irradiance measurements. In panel (b), ALADIN hindcast simulations and ground-based measurements are represented as colored areas and lines, respectively. The total height of each area or line represents the monthly average global irradiance, which is the sum of the direct (in yellow) and diffuse (in blue) components. In panel (c), ALADIN hindcast simulations of the seven aerosol types are represented as colored areas, while AERONET photometric measurements are depicted by thick black lines. As photometric measurements are only reliable in the absence of clouds in the direction of the Sun, they may not be representative of all-sky conditions. Hence, for consistency, monthly mean values derived from ALADIN hourly AOD simulations are limited to simulations coincident with measured hourly (diurnal) averages.

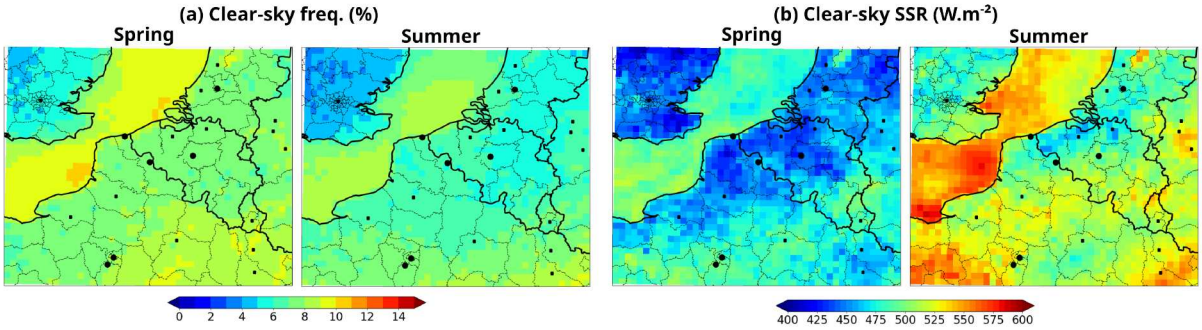

Figure S6. Seasonal averages over the period 2010-2020 of ALADIN daytime hourly hindcast simulations of clear-sky (a) frequency and (b) SSR in spring and summer.

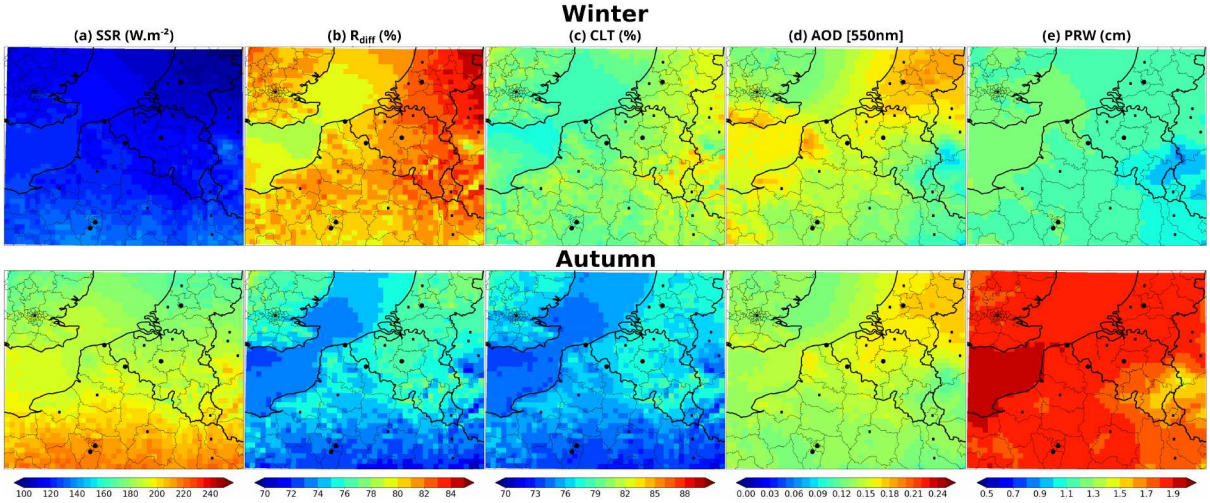

Figure S7. Seasonal averages over the period 2010-2020 in winter (upper figures) and autumn (lower figures) of ALADIN daytime hourly hindcast simulations under all-sky conditions of (a) surface solar radiation, (b) diffuse ratio ($R_{diff} = \frac{DHI}{GHI}$), (c) cloud fration, (d) AOD at 550 nm, and (e) precipitable water.

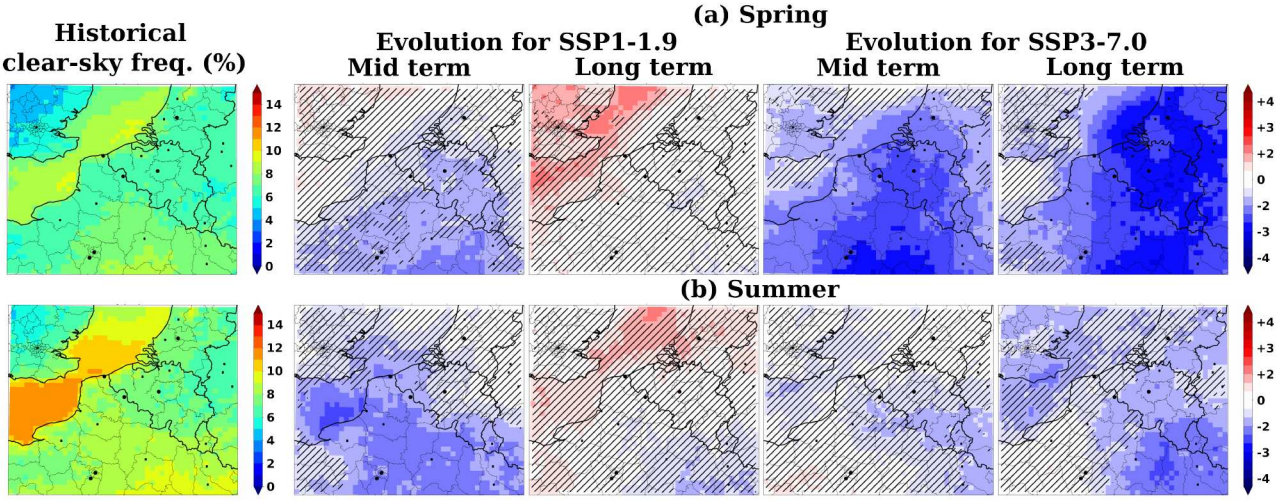

Figure S8. Future evolutions for CMIP6 scenarios SSP1-1.9 and SSP3-7.0 of the daytime clear-sky frequency (%) estimated from ALADIN simulations compared to the reference climate simulations over the period 2005-2014 (left panels) in (a) spring and (b) summer. Hatched areas correspond to areas characterized by a non-significant changes relative to a Student t-test with a significance level of 10%.

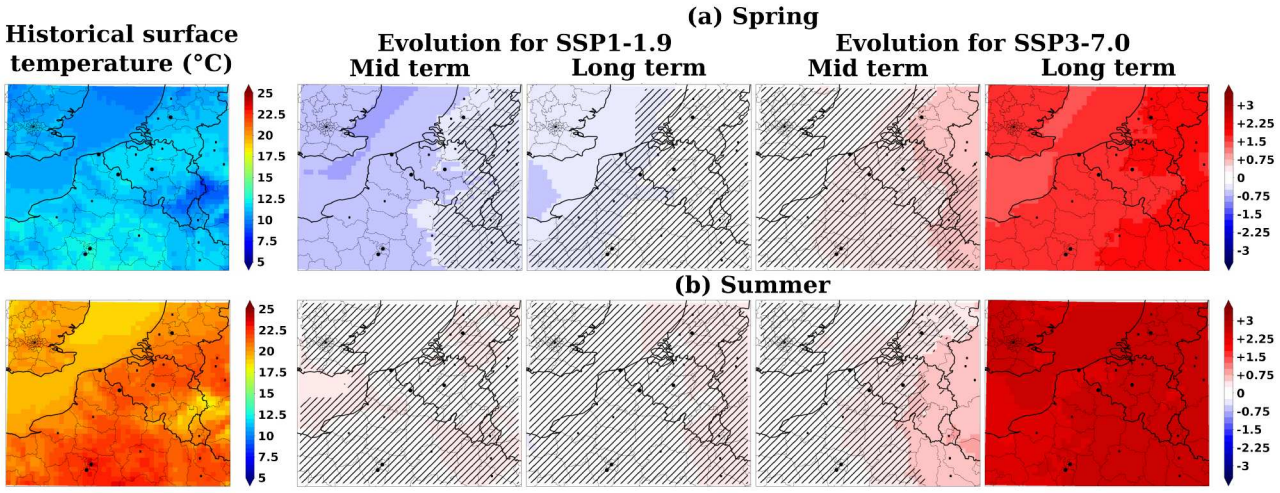

Figure S9. Future evolutions for CMIP6 scenarios SSP1-1.9 and SSP3-7.0 of the daytime surface temperature (°C) simulated by ALADIN compared to the reference climate simulations over the period 2005-2014 (left panels) in (a) spring and (b) summer. Hatched areas correspond to areas characterized by a non-significant changes relative to a Student t-test with a significance level of 10%.

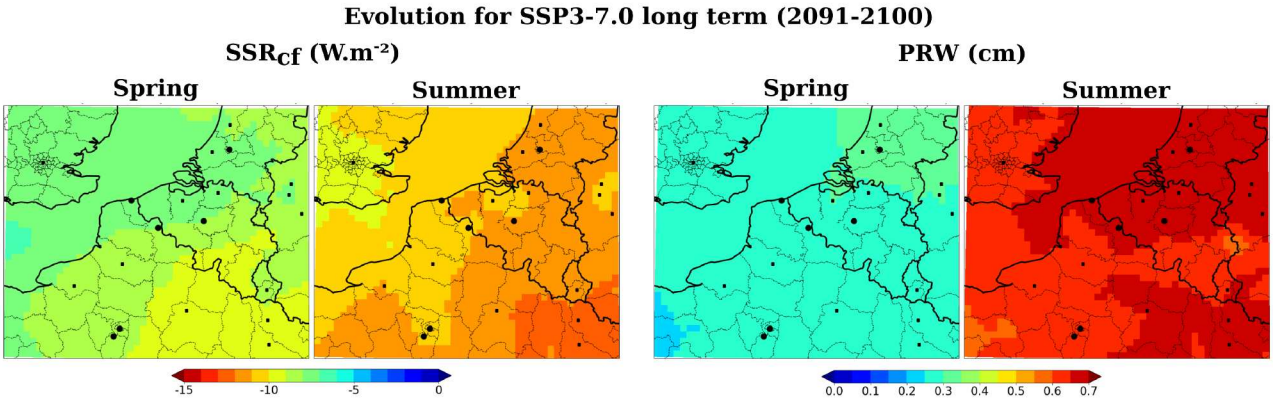

Figure S10. Future evolutions in spring and summer for CMIP6 scenario SSP3-7.0 of the daytime cloud-free SSR (SSR_{cf}) and precipitable water vapor content simulated by ALADIN compared to the reference climate simulations over the period 2005-2014 (left panels). Hatched areas correspond to areas characterized by a non-significant changes relative to a Student t-test with a significance level of 10%. Apart from their colorbars, these panels are identical to the rightmost panels of Figures 9-12c.

	Sulfate		**Nitrate**		**Ammonium**		**Organic**		**Black carbon**		**Total $\mathbf{PM_1}$ concentration** $(\mu g.m^{-3})$	
	Model	ATOLL	Model	ATOLL	Model	ATOLL	Model	ATOLL	Model	ATOLL	Model	ATOLL
Winter	0.7	1.5	2.6	5.1	0.8	2.2	1.3	5.7	0.5	1.4	**5.8**	**15.9**
Spring	0.8	1.1	6.8	5.2	2.0	2.1	1.1	4.1	0.4	0.7	**11.0**	**13.3**
Summer	0.8	1.2	3.8	2.1	1.1	1.3	1.0	4.8	0.4	0.7	**7.1**	**10.1**
Autumn	0.8	1.2	2.8	3.6	0.8	1.6	1.3	4.8	0.5	1.1	**6.1**	**12.2**
Overall	**0.8**	**1.2**	**4.0**	**4.0**	**1.2**	**1.8**	**1.2**	**4.9**	**0.4**	**1.0**	**7.5**	**12.9**

Table S1. Mean daytime PM_1 surface concentrations (in $\mu g.m^{-3}$), per season and on average over the period 2016-2020, of the different aerosol types simulated by ALADIN or measured by the ACSM and aethalometer from the ATOLL platform.

Mean aerosol optical depth at 550 nm									
		Total	**Sulfate**	**Nitrate**	**Ammonium**	**Organic matter**	**Black carbon**	**Sea salt**	**Desert dust**
HINDCAST	**2010-2020**	0.19	13.6	51.0	13.7	4.6	1.8	14.1	1.2
Historical	**2005-2014**	0.17	16.7	46.5	12.5	3.9	1.9	16.2	2.3
SSP1-1.9	**2045-2054**	0.14	6.4	56.3	15.3	2.2	0.3	18.1	1.3
	2091-2100	0.13	4.9	56.6	12.3	4.7	0.1	19.6	1.7
SSP3-7.0	**2045-2054**	0.20	8.4	55.0	15.0	3.0	0.9	15.7	1.9
	2091-2100	0.19	7.0	56.0	15.3	2.3	0.6	17.0	1.8

(a) Spring

Mean aerosol optical depth at 550 nm									
		Total	**Sulfate**	**Nitrate**	**Ammonium**	**Organic matter**	**Black carbon**	**Sea salt**	**Desert dust**
HINDCAST	**2010-2020**	0.14	18.4	44.1	11.8	6.1	2.2	15.4	2.2
Historical	**2005-2014**	0.13	22.6	41.6	11.0	6.3	2.6	14.6	1.4
SSP1-1.9	**2045-2054**	0.11	7.8	54.3	14.7	4.7	0.5	16.6	1.4
	2091-2100	0.10	6.1	55.7	15.1	4.3	0.3	17.0	1.6
SSP3-7.0	**2045-2054**	0.15	10.5	53.7	14.6	5.6	1.3	12.9	1.3
	2091-2100	0.15	8.9	55.8	15.3	4.9	1.0	13.0	1.1

(b) Summer

Table S2. Mean AOD at 550 nm over the BNF region and corresponding contributions (in %) of the different aerosol types simulated by ALADIN for *HINDCAST*, *HIST*, *SSP119* and *SSP370* datasets in (a) spring and (b) summer.

Δ AOD [550 nm]	-0.05	-0.04	-0.03	-0.02	-0.01	+0.01	+0.02	+0.03	+0.04	+0.05	+0.06	+0.07
Δ PRW (cm)	-0.5	-0.4	-0.3	-0.2	-0.1	+0.1	+0.2	+0.3	+0.4	+0.5	+0.6	+0.7
Associated $\Delta\mathbf{SSR_{cf}}$ ($W.m^{-2}$)	+8.5	+6.8	+5.1	+3.4	+1.7	-1.7	-3.4	-5.1	-6.8	-8.5	-10.2	-11.9

Table S3. Sensitivity of the surface solar irradiance, in $W.m^{-2}$, relative to changes in aerosol optical depth and precipitable water under clear-sky conditions. Results based on radiative transfer simulations presented in Chesnoiu et al. (2024b) for typical values of atmospheric parameters observed in Lille over the period 2010-2022.